

# Design and Optimization of an MB-OFDM Ultra-Wideband Receiver Front-End

Yanmei Li, Chang-Ching Wu, Alberto Sangiovanni-Vincentelli, and Jan M. Rabaey

Department of EECS, University of California, Berkeley

Email: {yanmei, jameswu, alberto, jan}@eecs.berkeley.edu

**Abstract**—The design of an MB-OFDM ultra-wideband receiver is challenging when we target power consumption minimization while providing enough robustness against the nearby wireless interference. We present an optimized receiver front-end design obtained by a systematic design space exploration technique based on the Platform-Based Design (PBD) methodology. At the system level, we investigate the interference effects and propose an approach to estimate the inter-modulation products introduced by receiver nonlinearities. We show how we map the system-level performance requirements to circuit-level platforms through an optimization process. We obtain a RF front-end consuming 10.8mW in a 0.13 $\mu$ m CMOS technology, which achieves a 22.3% savings of power compared to a manually optimized design.

## I. INTRODUCTION

As one of the most exciting evolutions of wireless communications, multimedia are able to travel over a wireless LAN. The wireless connectivity offers more flexibility and new potentials in consumer applications. The growing demands of wireless multimedia transmission raise more challenging requirements on wireless communications. Ultra-WideBand (UWB) is considered to be a compelling solution for short-range communications (1-10m), which is characterized by high data rates (e.g. hundreds of megabits per second), low power consumption, high robustness to multi-path fading, and low power transmission that allows it to coexist with other wireless technologies.

There are two competing UWB radios under consideration: the direct-sequence impulse radio and the Multi-Band Orthogonal Frequency Division Multiplexing (MB-OFDM) radio. The UWB spectrum released by the FCC spans from 3.1GHz to 10.6GHz. For the MB-OFDM UWB radio, as specified by the Multi-Band OFDM Alliance (MBOA) standard [1], the spectrum is divided into five band groups, each composed of 528MHz spaced frequency-hopping bands carrying OFDM signals. In this paper, we focus on the MB-OFDM UWB systems operating in the first band group (Mode I), which spans the frequency range from 3.1GHz to 4.8GHz.

Our goal is to design a low-power UWB receiver that should be sufficiently robust against nearby interference. Typically, UWB receivers operating in band group 1 will suffer from potential interference from standards such as 802.11a/b WLAN, WiMax, Bluetooth, and so on (Fig. 1). The interference could have significant impacts given the anticipated weak power levels of the UWB signal (maximum power spectral density is -41.3dBm/MHz). A strong narrow band interferer could be as much as 60dB above the UWB signal at the receiver antenna.

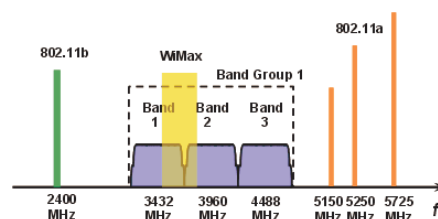


Fig. 1. Interference scenario around UWB band group 1.

This situation imposes challenging design requirements on the desensitization, linearity and dynamic range of a UWB receiver. Design challenges also come from the need for input impedance matching and gain flatness over the broad band (3.1-4.8GHz), the design of a broadband transmit/receive (T/R) switch, and so on. Traditionally, a complex analog/RF design such as this is carried out by trial-and-error and is rarely optimized. We believe that a systematic design space exploration is essential to obtain an optimal system and to improve the state of the art of wireless design technology.

In this paper, we present a UWB RF front-end design starting from system level analysis down to circuit implementation. In section II, we investigate the interference impacts at system level and propose an approach to estimate the inter-modulation products. In section III, we introduce the behavioral models developed at architectural level, that will be used to perform design space exploration based on the PBD methodology [2]. In section IV, low power front-end circuits are designed and their performance profiles are generated. In section V, a top-down process of mapping the system-level specifications to circuit platforms is conducted by optimization, and the results are reported.

## II. SYSTEM LEVEL ANALYSIS OF UWB RECEIVERS

To design a low power receiver, a critical task is trading off the system requirements, including nonlinearities, Noise Figure (NF), implementation loss, gain. Minimizing power consumption of a robust design implies the need of thorough investigation and accurate estimation of the interference influences on the receiver's performance.

An OFDM signal consists of the parallel transmission of several signals that are modulated at equally-spaced carrier frequencies  $\omega_n$  [3], i.e.:

$$x(t) = g_T(t + \phi) \sum_{n=-\frac{N}{2}}^{\frac{N}{2}} [i_n \cos((\omega_c + \omega_n)t + \psi) + q_n \sin((\omega_c + \omega_n)t + \psi)] \quad (1)$$

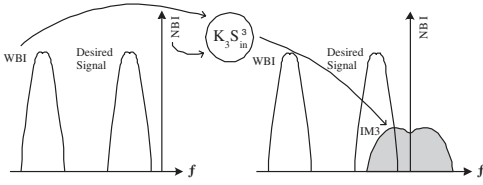


Fig. 2. XMD products of NBI (adjacent to the desired band) and WBI.

where  $N$  is the total number of OFDM sub-carriers,  $i_n$  and  $q_n$  are the real and imaginary parts of the baseband QPSK,  $\omega_c$  is the band center frequency,  $\phi$  and  $\psi$  are random phases.  $\omega_n = n \cdot \Delta\omega$ , where  $\Delta\omega$  is the subcarrier frequency spacing. With the constellation point  $c_n = i_n + jq_n$ , the corresponding complex envelope is  $g_T(t + \phi) \sum_n c_n e^{j\omega_n t}$ . If the OFDM symbol total duration is  $T$ ,  $g_T(t)$  is a rectangular function defined as:

$$g_T(t) = \text{rect}\left[\frac{t}{T}\right] = \begin{cases} 1, & -\frac{T}{2} < t < \frac{T}{2} \\ 0, & \text{elsewhere} \end{cases} \quad (2)$$

$$= 0, \quad \text{elsewhere} \quad (3)$$

### A. Estimation of Interference Inter-modulations

Suppose the MB-OFDM UWB receiver is operating in band 1, spanning the range from 3168MHz to 3696MHz. We classify the various interference into two categories: Narrow Band Interference (NBI), such as the ones introduced by 802.11a/b, and Wide Band Interference (WBI), such as the ones caused by other UWB transmitters. In UWB systems, since the transmitter and the receiver are not turned on simultaneously, the transmitter leakage is not a major interference source (as in WCDMA). The WBI mainly comes from other nearby UWB transmitters operating in different TFI (Time-Frequency Interleaving) patterns.

Due to the nonlinear behaviors of UWB receivers, the distortion products of these interferences could fall into the band of interest, degrading the system SNR. The inter-modulation distortion (IMD) products introduced by the second-order nonlinearity are usually mapped to bands far from the desired UWB signal passband. The third order term is responsible for most of the unwanted in-band IMD products. Considering the combination of two NBIs, since the in-band IMD products corrupt only a small fraction of sub-bands (e.g. 802.11a/b WLAN has a 20MHz bandwidth), we neglect their contributions to SNR degradation. We focus on the IMD products from NBI and WBI as well as from WBI and WBI. For those strong NBIs, we also consider their possible desensitization effects.

We model the NBI as a single-tone sinusoid signal  $S_{NBI}(t) = A_{NBI} \cos(\omega_{NBI} t)$ , and the WBI as an OFDM signal defined in (1) with the center frequency  $\omega_{WBI}$ . When the number of sub-carriers  $N$  is high, according to the central limit theorem, we hypothesize that the discrete time samples of an OFDM signal can be considered as zero-mean Gaussian random variables. Consequently, an OFDM WBI can be modeled as a cyclostationary Gaussian stochastic process.

Based on statistical signal processing, we derive the power spectrum density (PSD) of the distortion products [4]:

- Feed the interference signals into a nonlinear model (e.g. a third-order polynomial), and derive the analytical IMD products in time domain.

- According to the Wiener-Khinchin theorem, PSD is derived by taking the Fourier transform of the IMD autocorrelation function.
- The autocorrelation functions are simplified using the statistical properties of the uncorrelated random coefficients,  $i_n$  and  $q_n$  in (1).

Following this procedure, we obtained the PSDs for various interference cases [4]. For instance, as shown in Fig. 2, the interferences are WBI and NBI that is inside or adjacent to the band of interest. This case actually is cross-modulation distortion (XMD). Suppose the received power of WBI is  $\sigma_{WBI}^2$ , the single-sided PSD of XMD products is:

$$PSD_{IM3}(\omega) = \frac{9}{4} k_3^2 A_{NBI}^2 \sigma_{WBI}^4 T \cdot \sum_{l=-N}^N [(N - |l| + 1) \cdot \text{sinc}^2((\omega - (\omega_{NBI} + l \cdot \Delta\omega))T)] \quad (4)$$

### B. Two-tone Approach Adjusted for UWB

The interference effects on an MB-OFDM UWB system were also examined using Matlab simulations. A model of the transmission chain is built to generate the MB-OFDM UWB signal, the signal then passes through a nonlinear behavioral model. Subsequently, the output PSD is obtained by simulation and compared to our proposed estimation.

We also simulated the two-tone approach which is widely used to characterize nonlinearities in narrow-band systems. Given the power of two-tone ( $\omega_1, \omega_2$ ) input signals,  $P_{in1}$  and  $P_{in2}$ , the output-referred  $P_{IM3.out}$  at  $(2 \cdot \omega_1 \pm \omega_2)$  can be related to IIP3 as:

$$P_{IM3.out} = 2 \cdot P_{in1} + P_{in2} - 2 \cdot IIP3 + \text{Gain} [dB] \quad (5)$$

The system simulation results show good agreement to our analytical IMD calculations, while deviation exists if compared to the traditional two-tone approach. The two-tone IM3 estimation in (5) is determined by the interference power and IIP3, while the actual PSD simulation shows that the IM3 products depend also on the bandwidth and frequency locations of the interferences. Therefore, to provide accurate IMD estimations of UWB systems, proper adjustments should be made to the two-tone technique (5).

Take the case of NBI and WBI in (4) as an example. Given the interference band locations, the band overlap between their IM3 spectrum and the desired UWB band,  $BW_{in} = [\omega_{NBI} + \Delta\omega \cdot N_L, \omega_{NBI} + \Delta\omega \cdot N_H]$ , should be determined first. Suppose  $P_{IM3}^+$  is the total in-band IM3 power calculated from the  $PSD_{IM3}(\omega)$  in (4), we define the adjustment factor as  $\delta P_{IM3} = P_{IM3}^+ / P_{IM3.out}$ .  $\delta P_{IM3}$  does not vary when the power level of interferences changes. With almost no loss of accuracy, we make an approximation assuming that the power of function  $\text{sinc}^2(\omega - \omega_0)$  totally falls into the overlap bandwidth  $BW_{in}$  if  $\omega_0 \in BW_{in}$ . For the case of NBI and WBI in (4), we obtained the adjustment factor [4]:

$$\delta P_{IM3} = P_{IM3}^+ / P_{IM3.out} \simeq 8 \frac{\Omega}{N^2} \quad (6)$$

$$\Omega = \begin{cases} \frac{1}{2}(N - |N_H| + 1)(N - |N_H| + 2), & \text{when } N_L = -N, -N \leq N_H \leq 0 \\ (N + 1)^2 - \frac{1}{2}(N_L^2 + N_H^2 + N), & \text{when } -N \leq N_L \leq 0, N_H = N_L + N \\ \frac{1}{2}(N - N_L + 1)(N - N_L + 2), & \text{when } 0 \leq N_L \leq N, N_H = N \end{cases} \quad (7)$$

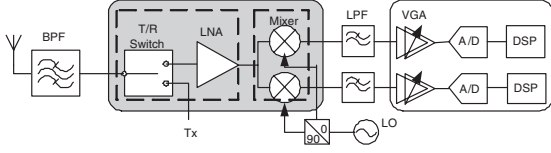


Fig. 3. Direct conversion UWB receiver architecture.

### C. UWB Receiver Specification

A pre-select Band-Pass Filter (BPF) is usually inserted between the antenna and the low noise amplifier (LNA) to limit the strong out-band interference that otherwise might desensitize the receiver. The  $i$ -th interference power at the receiver's input is  $P_{intf_i}^- = P_{intf_i} - A_{flt_i}$ . For an optimal receiver design, we should consider not only the attenuation capabilities ( $A_{flt}$ ), but also the insertion loss ( $IL_{BPF}$ ) of this BPF. The 1dB compression requirement ( $P_{1dB}$ ) is determined by the maximum interference to avoid the desensitization ( $P_{1dB} \geq \max_i \{P_{intf_i} - A_{flt_i}\}$ ). This also implicitly sets a constraint for the front-end IIP3. Here, we use the two-tone approach to estimate the various IM3 products  $P_{IM3(ij)}$ , with proper adjustments  $\delta P_{IM3(ij)}$  (in dB).

The noise contribution from the reciprocal mixing effects is neglected because the out-band interference is at a large frequency offset. The various third order IMD products,  $P_{IM3(ij)}$ , are the dominant contributors to  $P_{IM\_total}$ . To analyze the system budget and derive the linearity specifications, the following equations are used to estimate the effects of the front-end IIP3, sensitivity, noise figure ( $NF_{frnd}$ ), filter attenuations ( $A_{flt_i}$ ), filter insertion loss ( $IL_{BPF}$ ), and the receiver implementation loss  $IL_{RX}$  (sensitivity =  $-80.5\text{dBm}$  at bit rate  $R_b = 110\text{Mb/s}$  [1]):

$$\begin{aligned} &((-174 + 10\log_{10}(R_b) + IL_{BPF} + NF_{frnd}) + P_{IM\_total})[dBm] \\ &\leq -80.5\text{dBm} + 6\text{dB} - IL_{RX} - E_b/N_o \\ &IIP3 \geq \max_i \{P_{intf_i} - A_{flt_i}\} + 12\text{dB} \\ &P_{IM3(ij)} = 2P_{intf_i}^- + P_{intf_j}^- - 2IIP3 + \delta P_{IM3(ij)} \end{aligned} \quad (8)$$

In the presence of interference, we operate the receiver at 6dB above sensitivity.  $E_b/N_o$  is chosen to satisfy  $PER < 8\%$  for a 1024 byte packet.

Among the various narrow-band interferences, we should try to get rid of the large in-band NBIs (e.g. WiMax) to avoid the possible significant degradation of system performance. An efficient technique is interference detection and mitigation [5]. In our work, we assume that the large in-band NBIs are dealt with by dedicated techniques, and not taken into account when we perform the receiver budget analysis. The major interference sources under our consideration are WBIs and out-band NBIs. For instance, to estimate the dominant  $P_{IM3}$ , we use a WBI with power  $P_{intf_1} = -35\text{dBm}$  and an out-band NBI with power  $P_{intf_2} = -17\text{dBm}$ . In the later top-down optimization process, the front-end performance involved in (8) will be estimated by behavioral models, and the design requirements formulated by these relations will be automatically balanced. Therefore, we do not need to manually solve the equations and distribute the specifications to each building block.

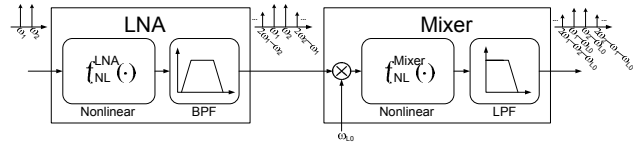


Fig. 4. A behavioral model of the UWB receiver front-end.

### III. BEHAVIORAL MODELS

In this work, a direct-conversion architecture is selected for the MB-OFDM UWB receiver, as shown in Fig. 3. We mainly focus on the receiver front-end design. The diagram of a behavioral model addressing nonlinearities and frequency responses is shown in Fig. 4. The coefficients of the model are fit by the circuit performances which are obtained from the circuit characterization.

A straightforward approach to estimate the front-end performance is to run the circuit-level simulation of the entire front-end circuits. The main purpose of building these behavioral models is to provide an abstract yet accurate representation of the corresponding building blocks so that the front-end performance could be quickly estimated, without running the intensive simulations at circuit level. Specifically, in the PBD flow, the high-level optimization is performed efficiently by employing the behavioral models, which therefore link the system specifications to circuit implementations.

A third order polynomial is used to model the nonlinear behaviors, represented as  $f_{NL}^{LNA}(\cdot)$  and  $f_{NL}^{Mixer}(\cdot)$  in Fig. 4:

$$\begin{aligned} V_{out}(t) &= a_1 \cdot V_{in}(t) + a_2 \cdot V_{in}^2(t) + a_3 \cdot V_{in}^3(t) \\ &\begin{cases} a_1 = \text{Gain} \\ a_2 = \frac{a_1}{V_{IIP2}} \\ |a_3| = \frac{4}{3} \cdot \frac{|a_1|}{V_{IIP3}^2} \end{cases} \end{aligned} \quad (9)$$

The coefficients  $a_1, a_2, a_3$  are related to the circuit performance,  $\text{Gain}$ ,  $V_{IIP2}$  (IIP2 in Volt),  $V_{IIP3}$  (IIP3 in Volt), which are all extracted from SpectreRF simulation of the LNA and the mixer circuits.

As the front-end behavioral model is a cascaded structure of the LNA block and the mixer block, the front-end performance can be approximated by analytical computation of the building block performance. For instance:

$$\begin{aligned} NF_{total} &\simeq NF_{LNA} + (NF_{Mixer} - 1)/\text{Gain}_{LNA} \\ 1/V_{IIP3\_total}^2 &\simeq 1/V_{IIP3\_LNA}^2 + \text{Gain}_{LNA}^2/V_{IIP3\_Mixer}^2 \end{aligned} \quad (10)$$

To obtain a more accurate performance estimation of the front-end, we developed a simulation-based approach. Since simulating RF behaviors in the time domain is computationally intensive, we conduct the behavior simulation in the frequency domain. Take the nonlinear model of LNA as an example. Suppose an input of two pure tones  $V_{in}(t) = A_1 \cos(\omega_1 t) + A_2 \cos(\omega_2 t)$  is plugged into a LNA as modeled in (9). Given  $V_{in}(\omega_1)$  and  $V_{in}(\omega_2)$ , the output responses at the various frequencies of interest can be directly computed. For instance, LNA outputs at  $\omega_1$  and  $(2\omega_1 - \omega_2)$  are:

$$\begin{aligned} V_{out}^{LNA}(\omega_1) &= V_{in}(\omega_1)(a_1 + \frac{3}{4}a_3|V_{in}(\omega_1)|^2 + \frac{3}{2}a_3|V_{in}(\omega_2)|^2) \\ V_{out}^{LNA}(2\omega_1 - \omega_2) &= \frac{3}{4}a_3V_{in}^2(\omega_1)V_{in}(\omega_2) \end{aligned} \quad (11)$$

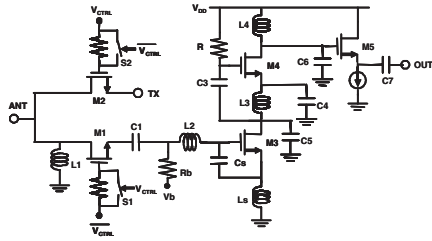


Fig. 5. Schematic of the T/R switch and the stagger tuning LNA.

Following the same principle, given the performances of the LNA and the mixer, we generalize the above tone-based computation for the cascaded model structure (Fig. 4) and derive the output spectrum of the overall front-end model. Knowing the input and output spectrum, the front-end nonlinear performances can be immediately estimated by probing the output spectrum at proper frequencies (after down-conversion). By comparing to the circuit-level simulations, it has been verified that these performance estimations are accurate enough for the system optimization purpose.

#### IV. DESIGN AND CHARACTERIZATION OF FRONT-END CIRCUITS

The RF front-end of the UWB receiver (Fig. 3) includes a T/R switch, a LNA, quadrature mixers and buffers. As the T/R switch and LNA dominate the overall noise performance of the receiver, low insertion loss of the T/R switch and low NF of the LNA are considered as essential design requirements. Besides that, these components must provide input matching over the broad operating band.

Based on our previous LNA design [6], we co-designed a T/R switch with a wideband LNA, as shown in Fig. 5. The passive components  $L1$ ,  $L2$ ,  $Ls$ , and  $Cs$  serve as the wideband input matching network. The T/R switch transistors  $M1$  and  $M2$  are also part of the matching network. The LNA employs the stagger tuning technique to achieve good gain flatness over a broad band. The first common-source stage consists of the transistor  $M3$  and the inductor  $L3$ , resonating at the lower frequency bound of the wide operating band.  $M4$  and  $L4$  serve as the second stage, resonating at the upper frequency bound. Our strategy to achieve power savings is to stack these two stages to make them share the bias current.

Following the LNA, quadrature mixers down-convert the RF signal to baseband. An output buffer ( $M5$ ) is added to LNA to prevent serious performance decay at high frequency caused by the mixer. To isolate the flicker noise and the second order intermodulation from the LNA, a DC blocking capacitor is inserted between the LNA and the mixer. A passive mixer (Fig. 6) is adopted for the advantage of wide bandwidth, low flicker noise, high linearity, and its zero DC power dissipation. A low-noise amplifier buffer ( $M3\sim M8$ ) is designed for the measurement purpose as well as further boosting the mixer gain.

Usually, circuit designers need to spend lots of time to manually determine the device sizings and bias conditions in order to achieve optimal circuit performance and low power consumption. Using the PBD flow, we leave this work to the optimizer, which will automatically decide the optimal sizings

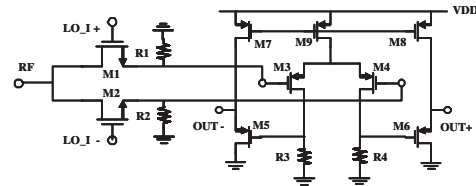


Fig. 6. Schematic of the Mixer and buffer.

and biasings. We performed circuit characterization using the SpectreRF simulator and an analog-PBD framework [7], which is capable of generating circuit configurations and extracting the various performance from the simulation results. The procedure of generating the circuit performance profile is summarized as:

- Construct a configuration space spanning by the design parameters such as length and width of transistors, parameters of inductors and capacitors, bias conditions, etc.
- Introduce constraints among the design parameters (e.g. bounding ranges for device sizes, proper operating conditions) to reduce the number of configuration variables and increase the characterization efficiency.
- By applying the configurations to a proposed circuit topology, a library of circuits with same topology are obtained. Run SpectreRF simulations to generate the performance space.

In this way, we obtain the manifold of performance that can be achieved by that circuit topology, where each point in the performance space corresponds explicitly to a set of design parameters. For both LNA (together with T/R switch) and mixers, we generated the performance profile including the critical circuit characteristics (e.g. gain), the important non-idealities (e.g.  $NF_{max}$ ,  $NF_{min}$ , IIP2, IIP3), and implementation costs (e.g. power, area). As an example, Fig. 7 shows a projection of the high-dimensional performance profile of LNA into  $NF_{max}$  and the current dissipation. It is shown that the achievable minimum  $NF_{max}$  is 3.4dB, and the minimum current consumption is around 4.2mA.

During the later top-down process, these performance profiles will be used to config the coefficients of the higher-level behavioral models. Consequently, using the behavioral models, the front-end optimization is restricted to visit only the feasible circuit performances (within the profile boundaries). With these performance profiles, another benefit is that automatic selection of the optimal design parameters will be performed quickly since no circuit simulation is required.

#### V. OPTIMIZATION AND RESULTS

With the support of the bottom-up circuit characterization, a top-down process of mapping the system-level specifications to circuit platforms is achieved by optimization. This is the *meet-in-the-middle* principle of PBD [2]. Knowing the performance profile of BPF based on the existing designs ( $IL_{BPF} = 1.0\text{-}1.8\text{dB}$ ), and typically  $IL_{RX}=2.5\text{dB}$ , we transformed the system design specifications to the performance requirements of the UWB receiver front-end. Then, an optimization process using the behavioral models mapped the requirements to the circuit platforms, as illustrated in

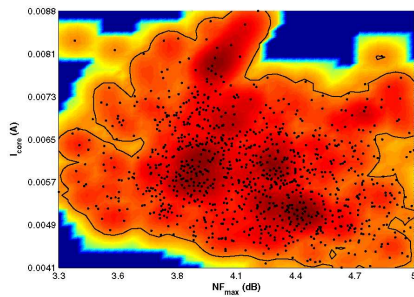


Fig. 7. A projection of LNA performance space. The area restricted by the boundary shows the achievable  $NF_{max}$  and current dissipation.

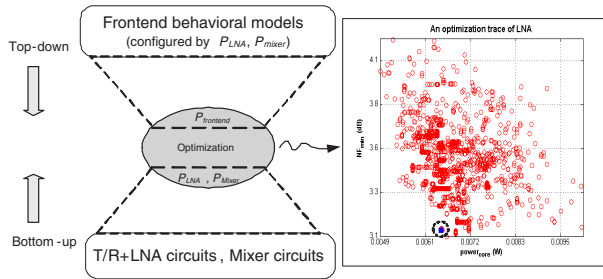


Fig. 8. The *meet-in-the-middle* optimization process. The performance space  $P_{LNA}$  and  $P_{mixer}$  are generated from the circuit characterization. The front-end performance  $P_{front-end}$  is evaluated by means of its behavioral model. On the optimization trace, the square marker (within the dashed circle) indicates the optimal  $NF_{min}$  and power consumption of LNA.

Fig. 8. Our optimization goal is to minimize the front-end cost function  $\mathcal{F}(power, area, NF, Gain)$  while satisfying the design requirements:

$$\min\{\mathcal{F}(\cdot) = \alpha_1 \cdot power + \alpha_2 \cdot area + \alpha_3 \cdot \Phi_1(NF) + \alpha_4 \cdot \Phi_2(Gain)\}$$

$$\text{s.t.} \quad \begin{cases} \text{Equ. (8)} \\ IIP3 \geq -23dBm \\ NF \leq 5.0dB, Gain \geq 24dB \end{cases} \quad (12)$$

where  $\Phi_1, \Phi_2$  are the penalty functions we defined for front-end NF and Gain, and  $\alpha_i$  reflects the contribution weights from different cost terms. We used a stochastic global optimizer, Simulated Annealing, which was customized for the PBD framework [7]. After optimization, an optimal performance vector of the front-end and the performance breakdown between the LNA and the mixer were provided. Correspondingly, with the support of the circuit performance space, the configuration parameters of all the circuits were obtained so that an optimal design of the UWB front-end circuits was immediately available. The simulated performance is compared to a manually optimized implementation (an industrial design provided by UMC), as shown in Table. I. A total power savings of 22.3% was achieved.

As shown here, using the PBD methodology, design optimization is efficiently performed using behavioral models at the system level and taking into consideration architectural constraints and implementation costs at the circuit level. With the circuit platforms, the feasibility of the optimization results is guaranteed, which is an essential and unique benefit associated with PBD. If the system design specification is modified, we just need to define a new optimization problem and run

the optimizer again, then a new optimal circuit solution will be available without running any circuit simulation.

TABLE I

Front-end perf.	Previous chip	Optim. design
<b>Band (GHz)</b>	3.1-4.8	3.1-4.8
<b>Voltage Gain (dB)</b>	23.0-27.6	27.5-29.2
<b>NF (dB)</b>	5.0-6.9	4.36-5.05
<b>IIP3 (dBm)</b>	-22.0 - -19.6	>-22.5
<b>P<sub>1dB</sub> (dBm)</b>	-34.3 - -31.8	>-34.6
<b>S11 (dB)</b>	<-7.5	<-11.8
<b>Power (mW)</b>	13.9	10.8
<b>Technology</b>	0.13 $\mu$ m	0.13 $\mu$ m

## VI. CONCLUSIONS

In this paper, we presented a systematic approach to design and optimize a RF front-end for MB-OFDM UWB receivers from system level to circuit level using the platform-based methodology. At system level, we investigated the interference impacts and performed statistical analysis to evaluate the inter-modulation products of various interferences. We also demonstrated how the narrow-band two-tone approach should be properly adjusted to be applied to UWB systems. For the receiver front-end, we presented the building blocks design and the platform characterization process. Finally, by mapping the system requirements to circuit platforms, we obtained a UWB front-end consuming 10.8mW with 1.2V voltage supply in a 0.13 $\mu$ m CMOS technology, achieving a 22.3% savings of power compared to a manually optimized industrial design. This optimal design is a joint contribution from the system-level analysis and specification balance, the development of low-power circuit topologies, and the automatic optimization of the circuit design parameters.

## ACKNOWLEDGMENT

The authors would like to thank Dr. Fernando De Bernardinis for his help on the Analog-PBD tool. They also thank United Microelectronics Corporation and the sponsors of the Berkeley Wireless Research Center (BWRC) for their great support, and thank the Gigascale Systems Research Center (GSRC) for funding this work.

## REFERENCES

- [1] A. Batra and et al., "Multiband OFDM physical layer proposal for IEEE 802.15 task group 3a," September 2004. [Online]. Available: <http://www.multibandofdm.org>
- [2] A. Sangiovanni-Vincentelli, "Defining Platform-based Design," *EEDesign of EETimes*, February 2002.
- [3] J. Proakis, *Digital Communications*, 4th ed. New York: McGraw-Hill, 2000.
- [4] Y. Li, J. Rabaey, and A. Sangiovanni-Vincentelli, "Analysis of interference effects in mb-ofdm uwb systems," in *IEEE Wireless Communications and Networking Conference (WCNC)*, April 2008.
- [5] S. Mishra, S. ten Brink, R. Madadevappa, and R. Brodersen, "Detect and avoid: An ultra-wideband/wimax coexistence mechanism," *IEEE Communications Magazine*, pp. 68-75, June 2007.
- [6] C.-C. Wu, A. Yen, Y. Cheng, and J.-C. Chang, "A switched gain low noise amplifier for ultrawideband wireless applications," in *IEEE 2007 Radio and Wireless Symposium*, January 2007.
- [7] F. D. Bernardinis, P. Nuzzo, and A. Sangiovanni-Vincentelli, "Mixed signal design space exploration through analog platforms," in *Proceedings of the 42nd Design Automation Conference (DAC'05)*, June 2005.